Supporting Information

Surface sulfidation toward highly active S/NiMoSe for superior alkaline hydrogen evolution

Xinyu Li, Huaiqing Yan, Yue Xiao, Fuxi Bao, Wen Guo*

School of Chemistry and Chemical Engineering/State Key Laboratory Incubation Base for Green Processing of Chemical Engineering, Shihezi University, Shihezi, 832003, China

*Corresponding author: wenguo@shzu.edu.cn

S1. Chemicals and Materials

Deionized water was used as the solvent in the experiments. Nickel (II) sulfate hexahydrate ($NiSO_4 \cdot 6H_2O$, Adamas, 98.5%), selenium dioxide (SeO_2, Macklin, 99%), potassium hydroxide (KOH, Macklin, 90%), sulfur powder (Sigma-Aldrich), sodium molybdate dihydrate ($Na_2MoO_4 \cdot 2H_2O$, 99%), Ethyl alcohol (A.R., ShengAo) and Hydrochloric acid (A.R., KESHI). Nickel Foam (NF: 99.98 % Ni) Purchased from Saibo Electrochemical Materials. All the received materials were used directly without any additional purification treatment, and throughout the entire experimental process, only AR-grade solvents were employed.

S2. Synthesis of NiMoSe electrocatalysts

NiMoSe was synthesized via a hydrothermal method. First, a piece of NF (1×1 cm) was sequentially cleaned in ethanol and hydrochloric acid using ultrasound to remove the surface oxide layer. The treated NF was then vacuum-dried at 60 °C overnight.

$NiSO_4 \cdot 6H_2O$ (80 mM), $Na_2MoO_4 \cdot 2H_2O$ (70 mM), and SeO_2 (90 mM) were dissolved in 60 mL of deionized water, followed by continuous magnetic stirring for 30 minutes to prepare a homogeneous solution. Subsequently, this solution and the pretreated NF substrate were transferred together into a 100 mL Teflon-lined stainless-steel autoclave. The autoclave was subjected to hydrothermal treatment at 200 °C for 12 hours. After the reaction, the system was allowed to cool naturally to ambient temperature. The solid product was then collected, thoroughly rinsed with ethanol and deionized water (three times each), and finally vacuum-dried at 80 °C overnight.

S3. Synthesis of S/NiMoSe electrocatalysts

The as-prepared NiMoSe precursor was subsequently subjected to controlled thermal annealing in a tube furnace, with sulfur powder as the sulfidizing agent and under a flowing nitrogen atmosphere. The temperature was programmed to rise to 350 °C at a heating rate of 5 °C·min^{-1} and maintained at this temperature for 2 hours, yielding the final sulfided product denoted as S/NiMoSe.

S4. Electrochemical measurements

All electrochemical measurements were conducted at room temperature using a CHI760E potentiostat (Chenhua Instruments, Shanghai). A standard three-electrode system was employed for the electrochemical tests. In this setup, the prepared nickel foam substrate loaded with S/NiMoSe (dimension: 1 cm × 1 cm) served as the working electrode, a Hg/HgO electrode (immersed in 1 M KOH solution) as the reference electrode, a graphite rod as the counter electrode, and a 1 M KOH aqueous solution as the electrolyte. All potential values were calibrated against the reversible hydrogen electrode (RHE) using the following equation:

$$E_{RHE} = E_{Hg/HgO} + 0.059 \times pH + 0.098\ V \qquad (S1)$$

Where E_{RHE} denotes the potential relative to the reversible hydrogen electrode, and $E_{Hg/HgO}$ represents the potential with respect to the Hg/HgO electrode.

Linear sweep voltammetry (LSV) curves were recorded at a scan rate of 2 mV·s^{-1} with 100% iR-compensation. Tafel slopes were subsequently derived from the LSV data using the following formula:

$$j = a + b\log(j) \qquad (S2)$$

The double-layer capacitance C_{dl} was determined via cyclic voltammetry (CV) measurements to evaluate the electrochemically active surface area (ECSA). The measurements were performed within a potential window of -0.23 V to -0.13 V versus the Hg/HgO electrode, with scan rates ranging from 20 $mV \cdot s^{-1}$ to 100 $mV \cdot s^{-1}$. ECSA was further calculated using the following formula:

$$ECSA = C_{dl}/C_s \times S_{geo} \qquad (S3)$$

Where C_s is the specific electrochemical double layer capacitance, and its value in alkaline medium is 0.040 mF cm^{-2}, and S_{geo} represents the geometric surface area of the working electrode.

The calculation formula for the ECSA-normalized current density j_{ECSA} is as follows:

$$j_{ECSA} = j_{geo} \times S_{geo}/ECSA \qquad (S4)$$

Where j_{geo} denotes the raw current density.

Electrochemical impedance spectroscopy (EIS) data were acquired over a frequency range of 100 kHz to 0.01 Hz, with an alternating current (AC) perturbation amplitude of 5 mV. Under HER conditions, the applied potential for measurement was set to -1.15 V versus the Hg/HgO electrode. The long-term electrochemical stability of the electrocatalyst was assessed via chronopotentiometric tests for the hydrogen evolution reaction, conducted at a current density of -100 $mA \cdot cm^{-2}$. The total duration of all stability tests was 41 hours.

S5. Material characterizations

The microstructure, morphology, and physical structure of the samples were characterized using field-emission scanning electron microscopy (FE-SEM, Zeiss Sigma 300) and transmission electron microscopy (TEM, America FEI Talos F200x). The phase structure of the synthesized samples was characterized using an X-ray diffractometer (XRD, Bruker D8 Advance, Germany) with Cu Kα radiation as the target source with a wavelength of 0.1518 nm, over a scanning range from 5° to 90° at a rate of 5°/min. The electrolyte collected after the stability test was first pretreated by filtration through acid digestion, followed by inductively coupled plasma optical emission spectroscopy (ICP-OES, Agilent 7800 MS, USA and Agilent Technologies 700 Series). The measurement was performed in parallel three times, and the average value was taken as the final result. The surface elemental composition and chemical states of the samples were characterized using an X-ray photoelectron spectrometer (XPS, ESCALAB 250Xi, Thermo Fisher Scientific, USA) equipped with a monochromatic Al Kα source (hυ = 1486.6 eV). All acquired photoelectron spectra were calibrated with reference to the C 1s peak at 284.8 eV for binding-energy correction. Raman spectroscopy measurements were conducted on the synthesized materials using a Raman spectrometer equipped with a 532 nm laser source (manufactured by Renishaw, UK).

S6. Details of in situ experiments

In-situ Raman spectroscopy measurements were conducted using a global Renishaw in

Via Qontor Raman microscope, with a 514 nm solid-state laser employed as the excitation source. The measurements were carried out in a custom-fabricated reactor, where the S/NiMoSe electrocatalyst-loaded electrode, Hg/HgO electrode, and platinum wire served as the working electrode, reference electrode, and counter electrode, respectively. The tests were performed in a 1 mol/L KOH electrolyte, and Raman spectra were acquired at various applied potentials. During the testing process, the generation of hydrogen bubbles induced spectral interference as the applied potential increased.

In-situ attenuated total reflection-Fourier transform infrared (ATR-FTIR) measurements were performed using a Bruker FOLI10-R-T FTIR spectrometer. A S/NiMoSe electrocatalyst-loaded electrode was used as the working electrode and immersed in a 1 mol/L KOH electrolyte. Prior to each hydrogen evolution reaction (HER) measurement, the background spectrum of the electrocatalyst electrode was collected at the open circuit potential (OCP). The HER-related ATR-FTIR measurements were conducted within a potential range of -0.1 V to -0.55 V (versus the reference electrode, typically Ag/AgCl). Specifically, the potential interval was set to 0.1 V for the lower potential region and 0.05 V for the higher potential region to capture more detailed spectral changes in the reactive potential range.

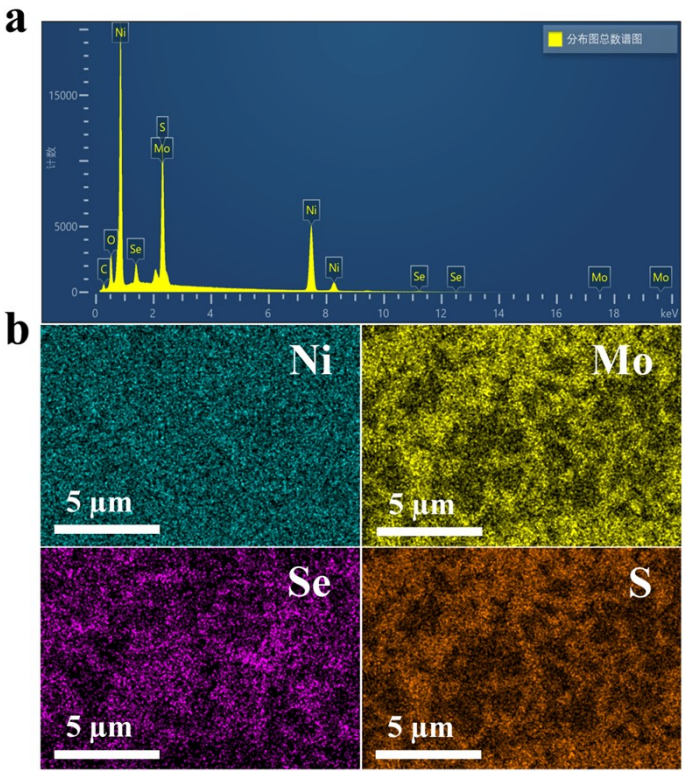

Fig. S1 (a) Contents of each element and (b) Elemental mapping images of S/NiMoSe.

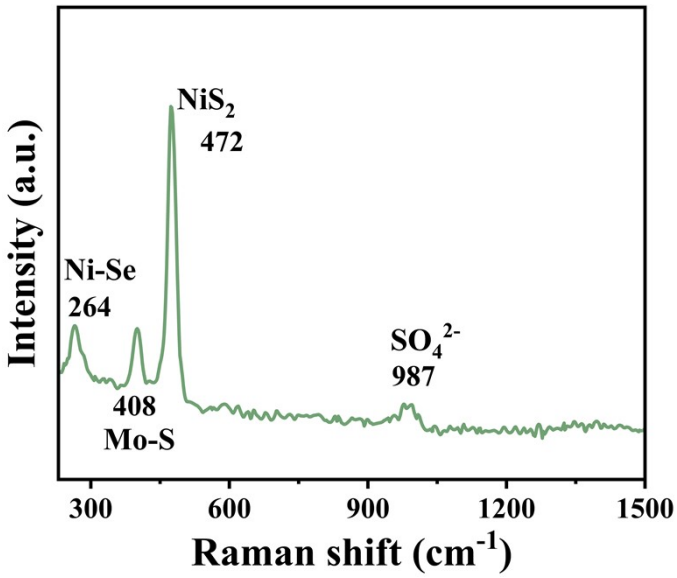

Fig. S2 Raman spectra of S/NiMoSe.

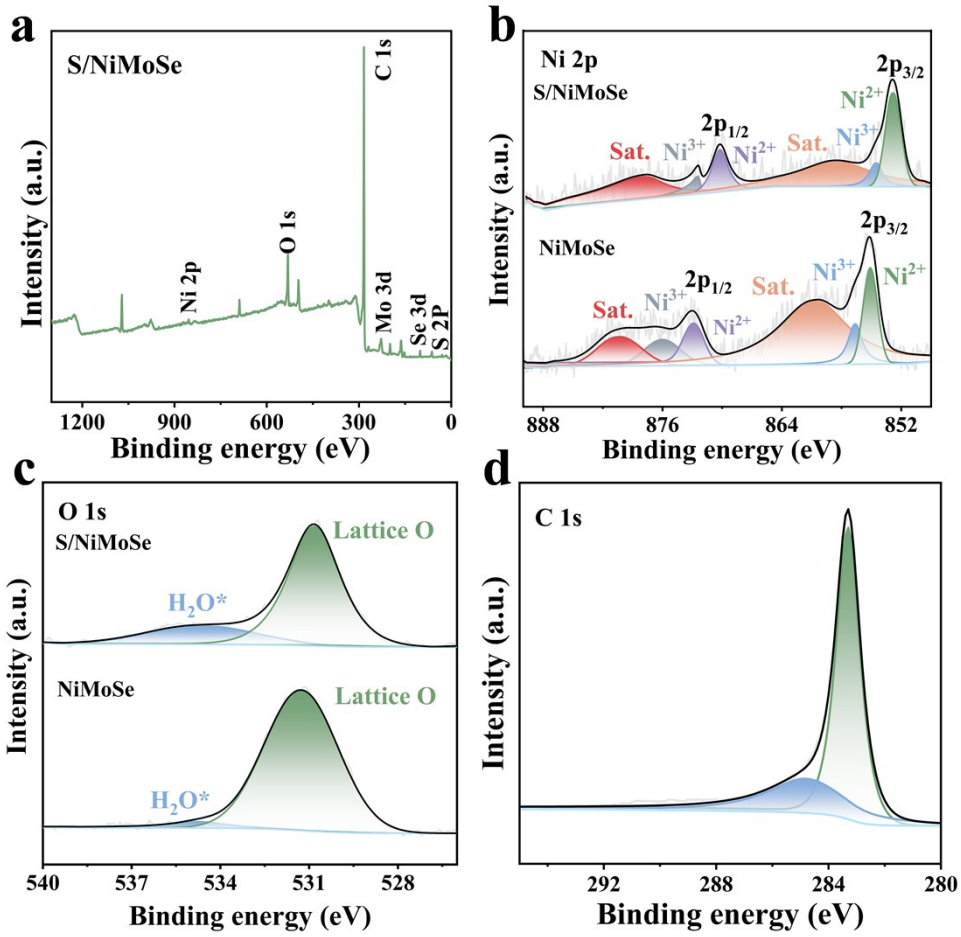

Fig. S3 (a) XPS survey spectra of S/NiMoSe; XPS spectra of (b) Ni 2p and (c) O 1s for S/NiMoSe and NiMoSe; (d) High-resolution spectrum of C 1s for S/NiMoSe.

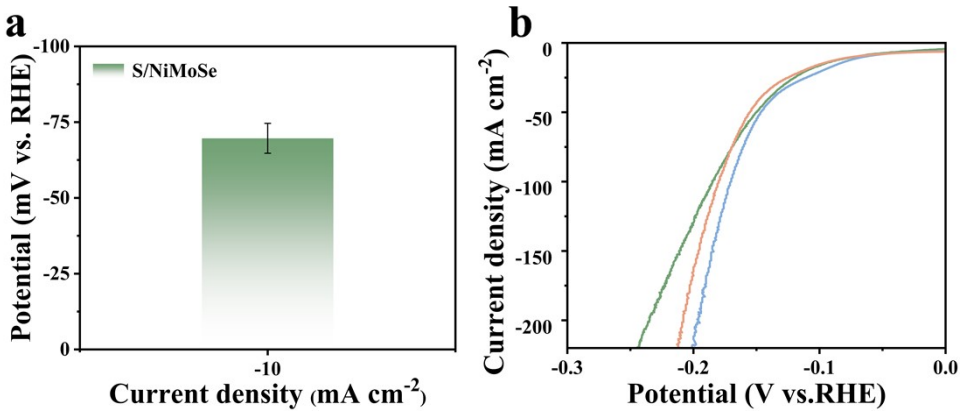

Fig. S4 (a) Error bars for S/NiMoSe represent the standard deviation of overpotentials at a current density of -10 mA cm^{-2} from three parallel tests, with a value of (-69 ± 4.9) mV, and (b) LSV curves of S/NiMoSe obtained from the three parallel test

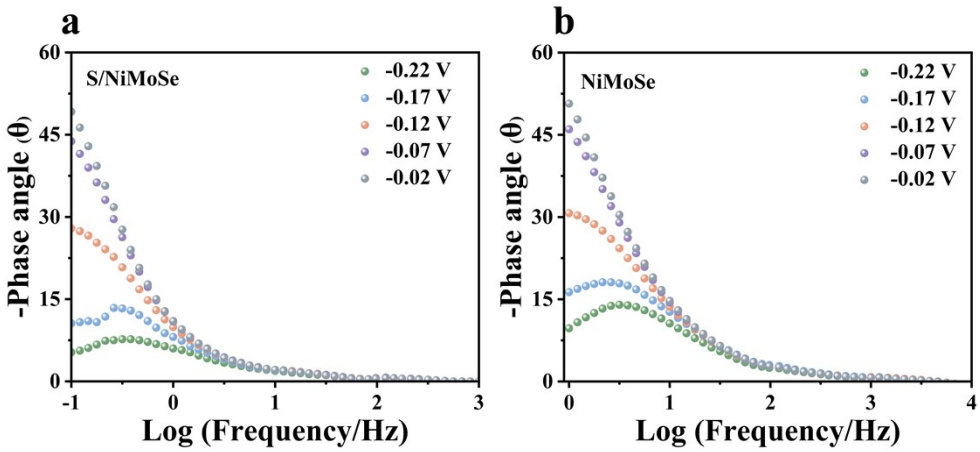

Fig. S5 Bode plots of (a) S/NiMoSe and (b) NiMoSe.

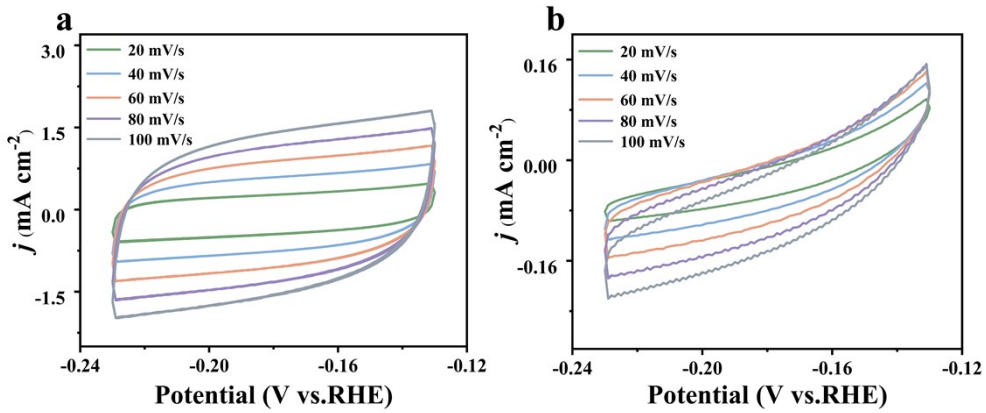

Fig. S6 CV curves at different scan rates for (a) S/NiMoSe, and (b) NiMoSe.

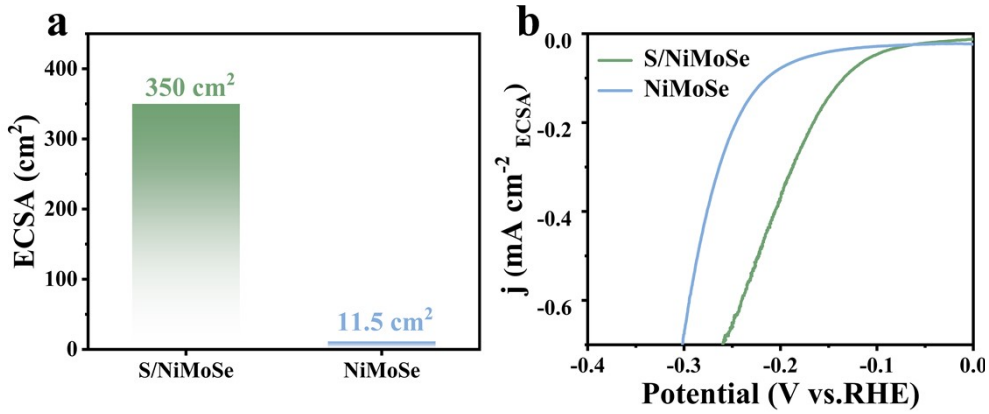

Fig. S7 (a) ECSA values and (b) ECSA-normalized LSV curves of S/NiMoSe and NiMoSe.

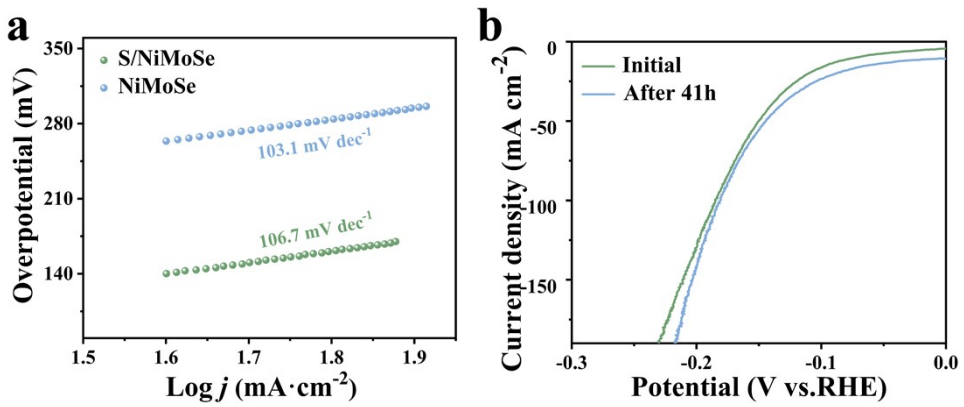

Fig. S8 (a) Tafel slopes; (b) LSV curves recorded before and after the 41 h stability test.

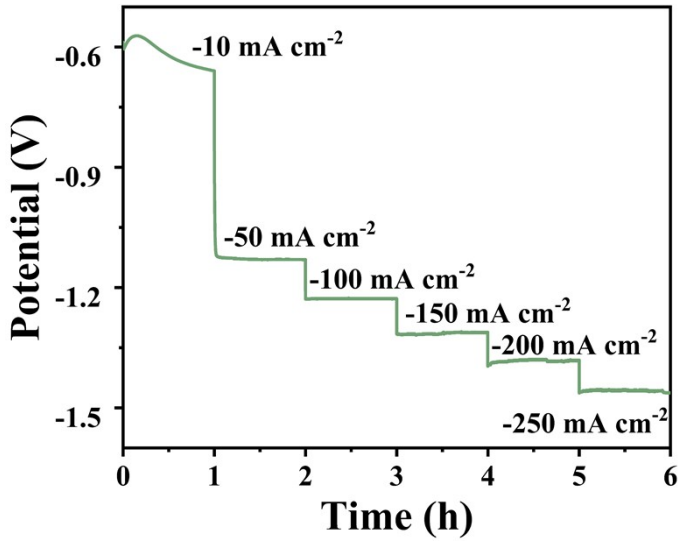

Fig. S9 The multi-step chronopotentiometric curve of the S/NiMoSe.

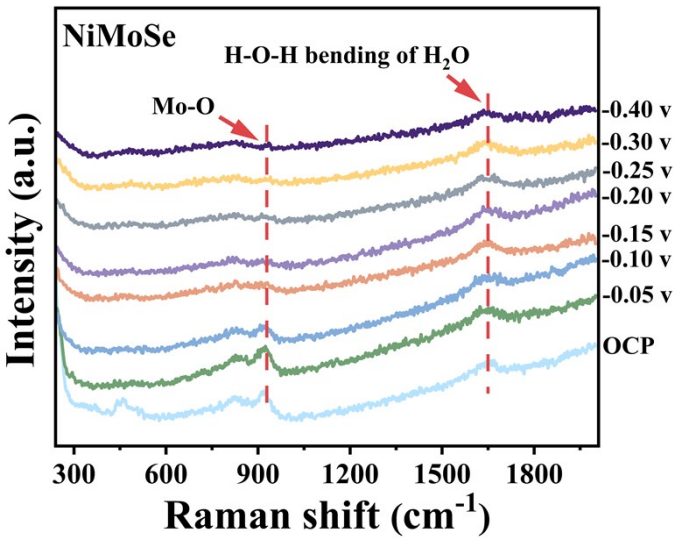

Fig. S10 In-situ Raman spectra of NiMoSe during HER process.

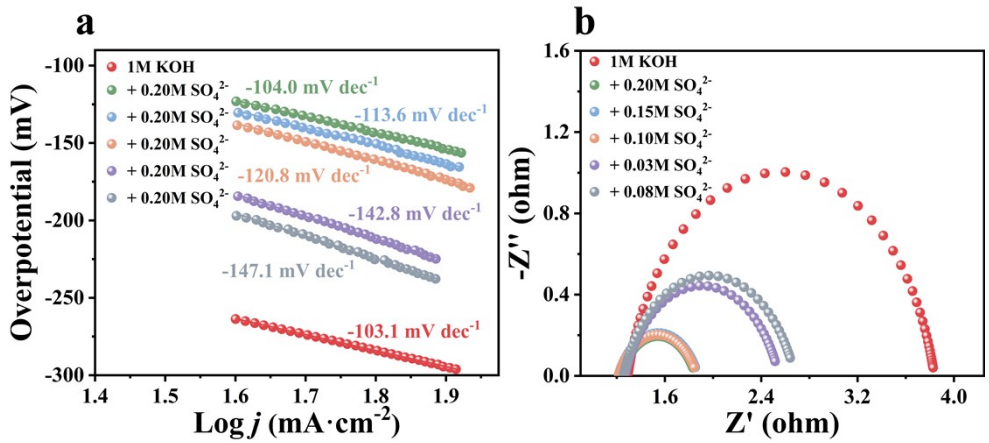

Fig. S11 (a) Tafel slope and (b) EIS Nyquist plots at -1.15eV of NiMoSe in 1M KOH with different concentrations of SO_4^{2-}.

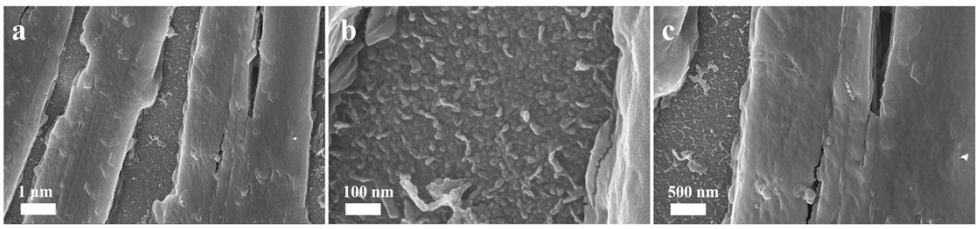

Fig. S12 SEM image of S/NiMoSe after 41 h HER stability test.

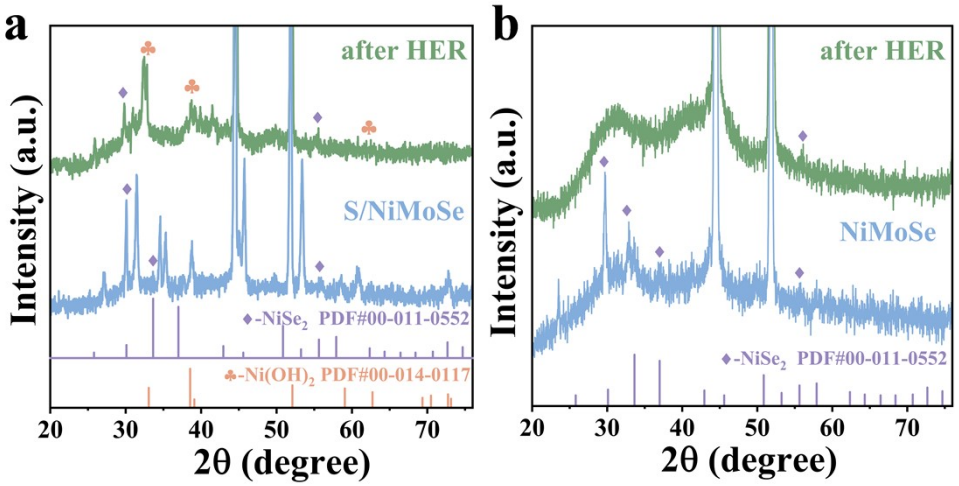

Fig. S13 XRD patterns of (a) S/NiMoSe and (b) NiMoSe before and after HER stability test.

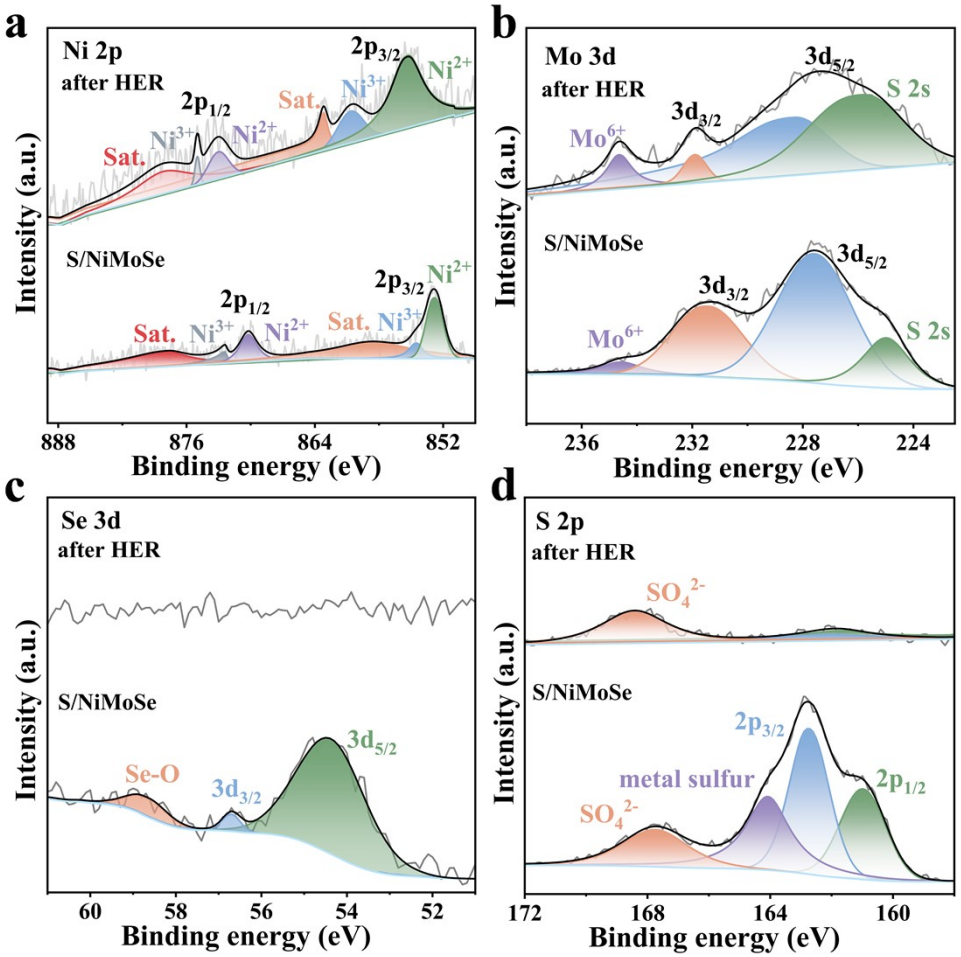

Fig. S14 XPS spectrum of S/NiMoSe after HER stability test (a) Ni 2p, (b) Mo 3d, (c) Se 3d, and (d) S 2p.

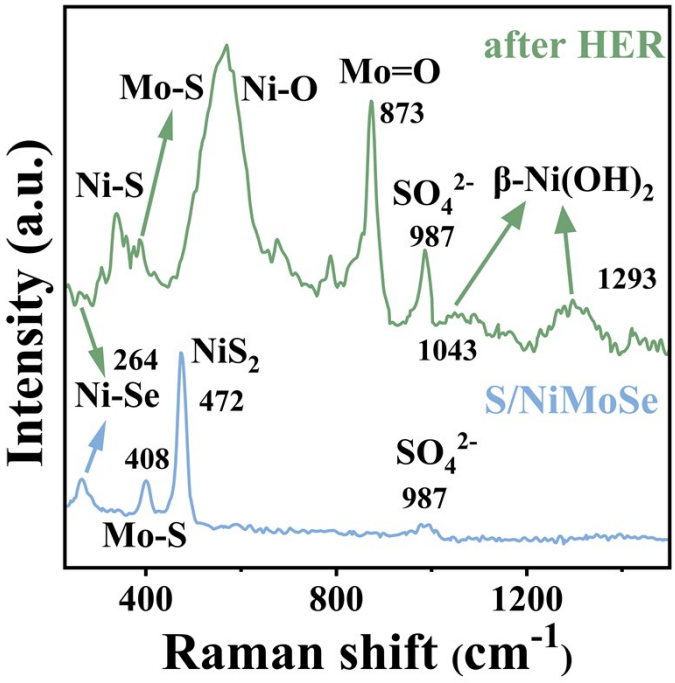

Fig. S15 Raman spectra of S/NiMoSe before and after HER stability test.

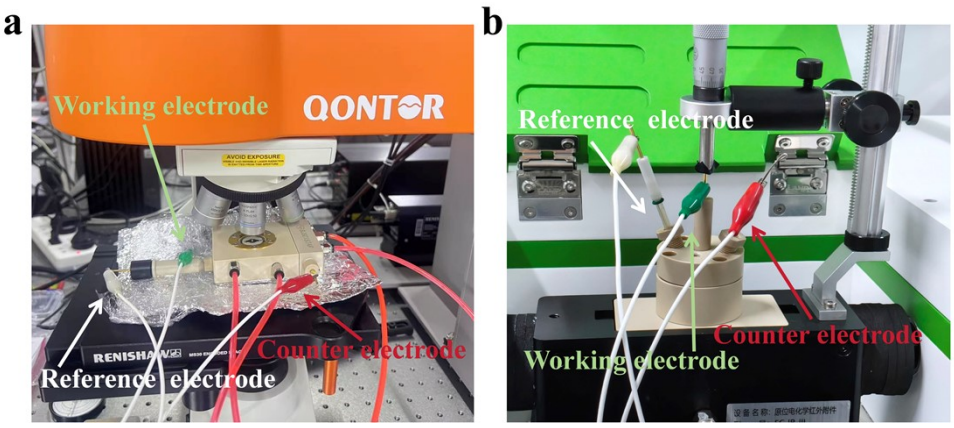

Fig. S16 (a) Photograph of the in situ Raman setup; (b) Photograph of the in situ FTIR setup.

Table S1 A comparison table of HER performance with the state-of-the-art electrocatalysts at -10 mA cm^{-2}.

Electrocatalyst	Overpotential (mV)	Electrolyte	Ref.
Se:CoS_{2-x}	-240	1.0 M KOH	[1]
MoS_2/NiS	-87	1.0 M KOH	[2]
Fe_2PdSSe	-104	1.0 M KOH	[3]
CNSSe	-82	1.0 M KOH	[4]
$[Mo_2O_2S_2(Se_2)(Se_x)]^{2-}$	-165	1.0 M KOH	[5]
Ni-Co-Se@NiS_2	-81	1.0 M KOH	[6]
$CoS_{2(1-x)}$ Se_{2x}@NC	-134	1.0 M KOH	[7]
$Ni_{0.25}Mo_{0.75}SSe$	-214	1.0 M KOH	[8]
Se(NiCo)S_x/$(OH)_x$	-103	1.0 M KOH	[9]
$MoS_{45.1}Se_{11.7}P_{6.1}$	-93	1.0 M KOH	[10]
$MoSe_2$/SnS	-374	1.0 M KOH	[11]
S/NiMoSe	-69	1.0 M KOH	This work

Table S2 Concentrations of S, Se, Mo and Ni dissolved in KOH electrolyte after 41 h HER stability test of S/NiMoSe at -0.38 V vs. RHE

Element content C_x (mg/L)	S	Se	Mo	Ni
after HER	190.29	40.79	62.31	4.26

Table S3 Concentrations of Se and Ni dissolved in KOH electrolyte after 41 h HER stability test of NiMoSe at -0.38 vs. RHE

Element content C_x (mg/L)	Se	Ni
after HER	61.59	9.66

References

1 Z. Shi, X. Qi, Z. Zhang, Y. Song, J. Zhang, C. Guo, W. Xu, K. Liu, and Z. Zhu, *Nanoscale*, 2021, **13**, 6890-6901.

2 X. Xu, W. Zhong, L. Zhang, G. Liu, and Y. Du, *International Journal of Hydrogen Energy*, 2020, **45**, 17329-17338.

3 K. C. Majhi and M. Yadav, *Energy & Fuels*, 2021, **35**, 12473-12481.

4 S. Huang, F. Meng, J. Dong, W. Zhuang, Z. Liang, C. Fan, X. Hou, and H. Wang, *Dalton Transactions*, 2025, **54**, 533-538.

5 A. Elliott, J. McAllister, L. Masaityte, M. Segado-Centellas, D.-L. Long, A. Y. Ganin, Y.-F. Song, C. Bo, and H. N. Miras, *Chemical Communications*, 2022, **58**, 6906-6909.

6 S. Jamali, M. A. Mohammadi, M. S. Yazdi, M. T. Noghani, A. Moghanian, M. Rezayat, and M. Morales, *Journal of Electroanalytical Chemistry*, 2024, **969**, 118527.

7 X. Xu, W. Zhao, L. Wang, S. Gao, Z. Li, J. Hu, and Q. Jiang, *Journal of Colloid and Interface Science*, 2023, **630**, 580-590.

8 R. Shwetharani, S. Mehta, B. Paswan, I. Kainthla, S. Dongre, A. Banerjee, and R. G. Balakrishna, *Fuel*, 2025, **394**, 135035.

9 C. Hu, L. Zhang, Z. J. Zhao, A. Li, X. Chang, and J. Gong, *Advanced Materials*, 2018, **30**, 1705538.

10 R. Bose, V. R. Jothi, B. Koh, C. Jung, and S. C. Yi, *Small*, 2018, **14**, 1703862.

11 A. Singh, J. Rohilla, M. S. Hassan, P. P. Ingole, P. K. Santra, D. Ghosh, and S. Sapra, *ACS Applied Nano Materials*, 2022, **5**, 4293-4304.